Journal of Alloys and Compounds 1007 (2024) 176452

Contents lists available at ScienceDirect

Journal of Alloys and Compounds

journal homepage: www.elsevier.com/locate/jalcom

Structural and luminescent properties of YSZ-YSH based ceramics depending on Zr/Hf ratio

Ekaterina V. Dementeva [a], Azaliya A. Shakirova [a], Kseniia N. Orekhova [a,*], Tatiana B. Popova [a], Maria A. Yagovkina [a], Aleksey I. Lihachev [a], Petr A. Dementev [a], Ivan D. Venevtsev [b], Anatoliy F. Zatsepin [c], Daniil S. Koshelev [d], Valentina V. Utochnikova [d], Boris E. Burakov [a], Maria V. Zamoryanskaya [a]

[a] Ioffe Institute, Saint-Petersburg, Russia
[b] Peter the Great St.Petersburg Polytechnic University, Saint-Petersburg, Russia
[c] Ural Federal University, Ekaterinburg, Russia
[d] Lomonosov Moscow State University, Moscow, Russia

ARTICLE INFO

Keywords:
ZrHfYO ceramics
Luminescence
Thermoluminescent dosimetry
Europium

ABSTRACT

Samples of crystalline cubic phased ceramics based on $(Zr_{1-x}Hf_x)_{0.82}Y_{0.17}Eu_{0.01}O_{1.91}$ with different contents of hafnium (x = 0; 0.21; 0.50; 0.77; 1) were synthesized. The synthesis conditions were chosen to avoid the possible formation of a minor tetragonal phase. The average grain size was 2–5 microns. The structural parameters of ceramics, their band gap, luminescent and thermoluminescent properties were studied depending on the hafnium content. It was shown that single-phase sample with calculated formula $((Zr_{0.77}Hf_{0.23})_{0.82}Y_{0.17}Eu_{0.1})O_{1.91}$ demonstrated the highest cathodoluminescent intensity upon excitation by electrons. It was found that thermoluminescent properties of ceramics with hafnium content of x = 0.50–0.77 range are prospective for application in thermodosimetry. The highest luminescence yield was observed in such samples.

1. Introduction

Zirconia-based materials demonstrate high mechanical, chemical and radiation stability. One of the unique features of zirconium oxide is that it has the ionic conductivity, which is associated with oxygen vacancies forming deep trap levels in the band gap of this material depending on their charge. All of these properties are related to the crystalline structure and chemical composition of zirconium oxide. At atmospheric pressure, there are three crystalline modifications of pure ZrO_2: monoclinic M, which is thermodynamically stable at temperatures below 1400 K; tetragonal T – forming at temperature from 1400 to 2570 K and cubic C – appearing above 2570 K and stable by melting point (2980 K) [1]. Zirconium oxide with structural modification C has the highest ionic conductivity and the highest oxygen vacancy content. In this case, Zr^{4+} cations form a conventional face-centered cubic lattice and oxygen atoms occupy tetrahedral interstices. Solid solutions of ZrO_2 with oxides of rare and alkaline earth elements (CaO, MgO, Y_2O_3, Sc_2O_3, etc.) may form stable cubic fluorite-type structure at room temperature. For the first time stable at room temperature cubic zirconia was obtained by Duwez et al. [2]. To stabilize the cubic phase of zirconium dioxide at room temperature it is necessary to add 8–20 mol% of trivalent or divalent ions. Single-phase cubic zirconia ceramic can be synthesized in the form of transparent samples.

In this regard, numerous studies are focused on cubic zirconia. Some investigations are devoted to the examination of luminescent properties of Y-stabilized zirconia ceramics (YSZ) doped with trivalent metal oxides: Dy_2O_3 [3], Er_2O_3 [4], Eu_2O_3 [5,6]. Doping of oxide materials with Eu^{3+} ions allows obtaining materials demonstrating intensive luminescence in the red optical range. In addition, the analysis of the emission spectra and its shape allows estimating Eu^{3+} local position in the material, and, consequently, the symmetry of the its matrix. [6–8]. In [8,9] it was demonstrated that a change in the crystal lattice affects the shape of Eu^{3+} spectrum. In [10] it was shown that Eu^{3+} spectra are sensitive to the excitation method and that luminescence bands referring to transitions from higher energy levels are observed in cathodoluminescence spectra than in photoluminescence. There is an active discussion about the crystal structure features and the charge carrier traps design in these materials depending on doping or precursor preparation and synthesis

* Corresponding author.
E-mail address: orekhova.kseniia@gmail.com (K.N. Orekhova).

https://doi.org/10.1016/j.jallcom.2024.176452
Received 17 June 2024; Received in revised form 21 August 2024; Accepted 9 September 2024
Available online 10 September 2024

conditions [6,11–13]. Thermodynamic properties of YSZ are prospective for the use as thermal barrier coatings [13,14] and other high temperature applications [15].

Thermoluminescent properties of YSZ doped with various trivalent metals: Eu [16], Er [17], etc. are also of great interest. Trivalent ions of rare earth elements may also stabilize cubic zirconia and increase content of oxygen vacancies. This leads to the formation of traps with an activation energy more than 0.5 eV at high concentration. Therefore, this material is promising for the use as sensors in thermoluminescent dosimetry. The presence of deep traps in such sensors is necessary to prevent the release of charge carriers at room temperature.

In papers devoted to the study of traps in zirconium and hafnium oxides, it is stated that oxygen vacancies act as traps. However, these studies propose different mechanisms of charge localization and values of trap activation energies. Traps in monoclinic HfO_2 have been investigated in a number of works. For example, in [18–20], a trap-associated tunneling process with $E_a \approx 0.4$ eV was discovered. In [21], it was shown that the thermal energy of an oxygen vacancy in monoclinic HfO_2 is 1.25 eV; in [22], it was shown that in lanthanum-doped hafnium oxide, the activation energy calculated using the Frenkel model is 0.8 eV, and the thermal energy calculated using the Nasyrov–Gritsenko model is 1.25 eV. Traps with an activation energy of 0.22 eV were observed in monoclinic ZrO_2 [23]. In orthorhombic $Zr_{0.5}Hf_{0.5}O$ it was shown [24] that the thermal energy of traps depends on the charge state of the oxygen vacancy and varies from 0.4 eV to 1.8 eV.

Stabilization of ZrO_2 and HfO_2 with the addition of trivalent ions in cubic phase occurs, among other things, due to the formation of oxygen vacancies. In [25], it was shown that negatively charged oxygen vacancies are predominantly associated with tetravalent ions. If comparing the energy positions of the defect levels calculated using the Kohn-Sham single electron model in [26] for HfO_2 and in [24] for $Zr_{0.5}Hf_{0.5}O$, it is evident that the presence of hafnium leads to a significant shift in the vacancies energy levels position in the forbidden zone. Accordingly, the dependence of the thermoluminescent properties of the oxides on the ratio of Zr^{4+} and Hf^{4+} content should be expected.

Possible application of thermoluminescent zirconia-based dosimeters for the use at high doses of radiation including high-energy particles was demonstrated before [27,28]. Zirconia irradiation by alpha particles causes neutron generation and part of the energy related to neutrons is not absorbed by zirconia matrix. In a contrast the hafnium, which has five stable isotopes (^{176}Hf, ^{177}Hf, ^{178}Hf, ^{179}Hf, ^{180}Hf) absorbs neutrons with high efficiency. This feature of cubic hafnia ceramic is very important for development of dosimeters detecting high-energy fluxes of ionizing radiation.

Hafnium is a close chemical analogue of zirconium. Cubic hafnia is stabilized through doping with trivalent metals too. Hafnium dioxide and ceramics based on cubic stabilized hafnia (YSH) were studied in terms of thermal stability [28–31], scintillation [32] and thermoluminescent properties [33] depending on dopants or synthesis conditions. Traps in thin films of HfO_2 and $Hf_xZr_{x-1}O_2$ are widely studied [34–37], but these studies did not cover massive ceramic samples. Ceramics based on a mixture of hafnia-zirconia are prospective for further research. The effect of YSZ/YSH ratio on basic ceramic properties is under consideration [38,39].

The aim of this work was to synthesize and study the structural, optical and thermoluminescent properties of ceramics based on single-phase zirconia-hafnia stabilized with yttrium and activated with Eu^{3+} ions.

2. Synthesis of ceramics and research methods

Starting precursors were obtained using co-precipitation technique from common aqueous solution. This method is the most economically feasible and acceptable for adoption by industry. Aqueous solutions of $ZrO(NO_3)_2$*2 H_2O, $HfClO_2$, $Y(NO_3)_3$, $Eu(NO_3)_3$ were prepared and filtered. The purity of the starting materials was 99.9 %. In order to make calibration 50 ml portion of each solution was used for precipitation by ammonium hydroxide. The precipitates obtained were washed by distilled water, dried for 12 hours at 150℃ in air and then calcined for 80 minutes at 800℃ in air. The weight of obtained oxide powders were recalculated for content of Zr, Hf, Y and Eu in respective solutions.

Five different blends of ceramic $(Zr_{1-x}Hf_x)_{0.82}Y_{0.17}Eu_{0.01}O_{1.91}$ were finally synthesized. In all cases the yttrium content was fixed to 0.17 formula unit taking into account that this amount stabilizes cubic phase of zirconia and hafnia according to reported data [40]. The europium content was also fixed to 0.01 formula unit because this concentration does not affect stability of cubic structure, but efficient enough for intensive luminescence emission. The hafnium content, *x* were selected: 0; 0.25; 0.50; 0.75; 1.

Precursor powders were ground in an agate mortar and pressed into tablets with a diameter of 8 mm under a pressure 10 MPa. Pellets obtained were sintered in air at temperature 1500°C for 3 hours. Fragments of ceramic samples were placed in acrylic resin, polished by 2000 grit SiC polish paper and coated by carbon. Similar polished samples but without carbon coating were used for atomic force microscopy. Ceramic plates with 8 mm in diameter and a thickness ≤ 1 mm were prepared in order to carry out thermoluminescence and photoluminescence studies.

The elemental composition of the samples was examined by electron probe microanalysis (EPMA) using CAMEBAX electron probe microanalyzer equipped with four X-ray wavelength spectrometers. The analysis was carried out with the following parameters of the electron beam: energy U = 20 keV, absorbed current I = 15 nA, beam diameter d = 2 μm. Analytical Lα lines for all elements were selected for analysis. Metallic zirconium (for Zr), metallic hafnium (for Hf), compounds of $Y_3Al_5O_{12}$ (for Y) and $EuPO_4$ (for Eu) were used as standards. Oxygen content was calculated according to stoichiometry. The elemental composition was measured in several (at least five) randomly selected areas of the samples. The average elemental composition of the samples was calculated. The error of the measurement technique was 10 % arb. for europium; 2 % arb. for the remaining elements [41].

Cathodoluminescence (CL) spectra, and decay kinetics for the most intense CL band were obtained for all synthesized ceramics on the same CAMEBAX electron probe microanalyzer, additionally equipped with an optical spectrometer. CL spectra of the samples were obtained in the wavelength range λ = 350–800 nm under the following conditions: electron beam energy U = 20 keV, absorbed current I = 50 nA, and electron beam diameter d = 5 μm. CL kinetics measurements were carried out with an electron beam diameter of 40 μm, since measurements with a smaller diameter lead to a larger scatter of the determined parameters [42].

All samples were studied by X-ray diffraction analysis (XRD). NaCl powder was used as an internal standard to determine the structural parameters of the samples. Measurements were carried out on a D2 diffractometer (Bruker, Germany) (λ = 1.5406 Å, 30 kV, 10 mA) equipped with a camera PSD detector LENXEYE.

Electron backscattered diffraction (EBSD) studies were carried out on a JSM 7001 F scanning electron microscope (JEOL, Japan) equipped with an HKL Nordlys EBSD Detector (Oxford Instruments, England). The sample was irradiated with an electron beam with an energy of 10 keV at an angle of 70° to the normal. When scanning with an electron beam along the surface of the sample, a diffraction pattern was recorded at each point, and based on the results of automatic decoding, the orientation of the ceramic grain was determined [43]. The scanning area size was 200×200 μm, scanning step was 1 μm. Surface preparation was carried out by polishing with an argon ion beam using a 1061 SEM Mill (Fischione, USA). EBSD signal maps were obtained and grains in the region of interest were visualized.

The surface topography was studied using an NTegra-Aura atomic force microscope (NTMDT-SI, Moscow, Russia) using standard silicon probes of the NSG-11 type (stiffness ~ 4 N/m, characteristic curvature radius of the probe tip ~ 10 nm). The measurements were carried out in semi-contact mode in air.

Optical absorption spectra were obtained for all samples using a Lambda 35 spectrophotometer.

The optical radiation quantum yield was measured on a Horiba FluoroMax Plus spectrofluorimeter with an integrating sphere. To increase the surface of interaction with light, the ceramics were ground in an agate mortar. The resulting powder was placed between two quartz glasses. In all measurements, it was controlled that the area of the irradiated sample was no less than the area of the optical beam exciting the radiation. The quantum yield values for the excitation of the $^7F_0$-$^5L_6$ and $^7F_0$-$^5D_2$ optical transitions were obtained for all samples.

Photoluminescence spectra and excitation spectra were obtained on a Horiba Fluorolog 3 spectrofluorimeter (Jobin Yvon) equipped with a 450 W xenon lamp and a characteristic signal-to-noise ratio of more than 20,000:1.

Thermoluminescence (TL) curves were measured in vacuum. The complete procedure was as follows: firstly, the sample was heated up to 573 K to clean the surface and release the traps; secondly it was cooled down to 77 K, irradiated with X-rays (continuous spectrum from tungsten anode X-ray tube at 40 kV and 10 mA) for 5 minutes; after a 10-minute pause the sample was heated at a constant rate of 0.25 K/s up to 573 K and thermoluminescence was recorded directly by the Hamamatsu H8259 photon counting head which has a sensitivity range from 180 to 650 nm and a dark count rate less than 10 counts per second. For each sample, measurements were taken over a large area, approximately equal to one square centimeter. The positioning of the samples was identical, which ensures sufficient reproducibility of the results.

3. Results and discussion

3.1. Composition and structural parameters

The average elemental composition of the samples from EPMA is presented in Table 1. The measured element content corresponds to originally designed composition; the deviation from the planned composition did not exceed the error limits of the measurement method for all samples. The name of the samples reflects the value of hafnium content, x.

XRD patterns were obtained for all samples (Fig. 1). It was shown that in all samples the dominant phase is the cubic phase (PDF 01–077–2286). Sample 0-Hf is monophasic and has no impurities of other phases, samples 0.21-Hf and 0.50-Hf have traces of the tetragonal phase (PDF 01–082–1245), in samples 0.77-Hf and 1-Hf a tetragonal phase with a content of about 1–2 % wt. is present. It was shown that additional annealing for 3 hours at a temperature of 1500°C leads to the disappearance of the minor phase. The coherent scattering region for each sample was determined and its size was shown to exceed 600 nm.

The lattice constant was determined for each sample and the dependence of the lattice constant on the x was obtained. It was shown that the lattice constant changes linearly with changes in the composition of the ceramic according to the following law: $a(x) = 5.148 - 0.0177x$, (Fig. 2). These results confirm the formation of a solid solution.

Table 1
Elemental composition of samples measured by EPMA, atomic concentrations relative to metals are given.

Sample		Element content, form. un			
Name	Hafnium content, x	Hf	Zr	Y	Eu
0-Hf	0±0.01	0	0.80±0.02	0.185 ±0.004	0.012 ±0.001
0.21-Hf	0.21±0.02	0.18 ±0.04	0.66±0.01	0.149 ±0.004	0.010 ±0.001
0.50-Hf	0.50±0.01	0.40 ±0.01	0.40±0.01	0.187 ±0.004	0.013 ±0.001
0.77-Hf	0.77±0.01	0.61 ±0.01	0.186 ±0.004	0.194 ±0.004	0.014 ±0.001
1-Hf	1.0±0.02	0.78 ±0.02	0	0.207 ±0.004	0.012 ±0.001

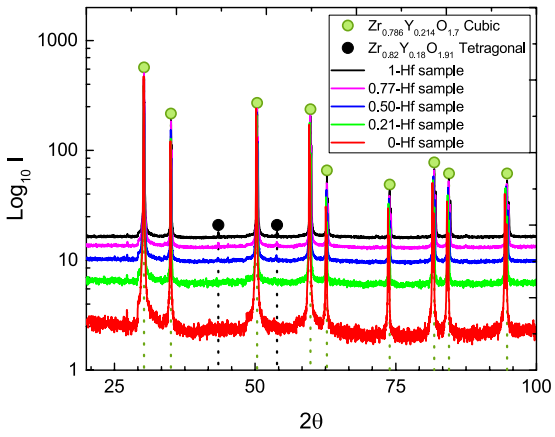

Fig. 1. XRD curves obtained for all samples. The figure also shows the reflections corresponding to the card of cubic ZrYO (PDF 01–077–2286) (green circles) and tetragonal ZrYO (PDF 01–082–1245) (black circles).

Atomic radius of Zr^{4+} is larger than of Hf^{4+} [44] (73 pm and 72 pm, respectively). Solid solution single phase ceramics of mixed oxides composition obeys Vegard's law, therefore the lattice constant decreases linearly with Hf content increase. It has been previously observed for other Zr-Hf single phase solid solutions [45,46].

It can be seen that the lattice constant for the 0.21-Hf sample deviates most from the linear approximation, which is most likely due to the lower Y content relative to the other samples.

Grain size distributions were studied using the combination of EBSD and AFM techniques. This combination was chosen due to the specific application of each method. Initial characterization of the surface by AFM showed that the surface of the samples is very rough (Fig. 3). It mainly consisting of large grains of 2–8 μm in size (indicated by arrows in Fig. 3). In addition, the space between large grains is filled with smaller grains with a characteristic size of 100–400 nm. The AFM method is poorly suited for studying such highly rough surfaces on a large scale. Therefore, in addition to the AFM studies, an EBSD study was carried out.

Using the EBSD technique, the grain size distributions were obtained for all samples (Fig. 4). It was shown that ceramics consists of grains with a size of 2–10 microns with a prevailing size of 4 microns (Fig. 4b). Grains with a size of 100–400 nm probably are not observed by XRD because they, being differently oriented, are densely located in the areas between the larger ones.

Thus, during the initial characterization of the samples, it was shown

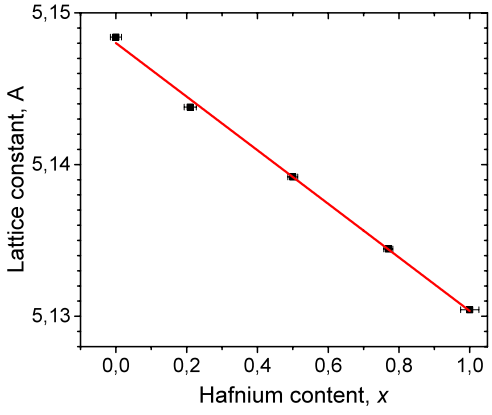

Fig. 2. Lattice constant versus hafnium content, x.

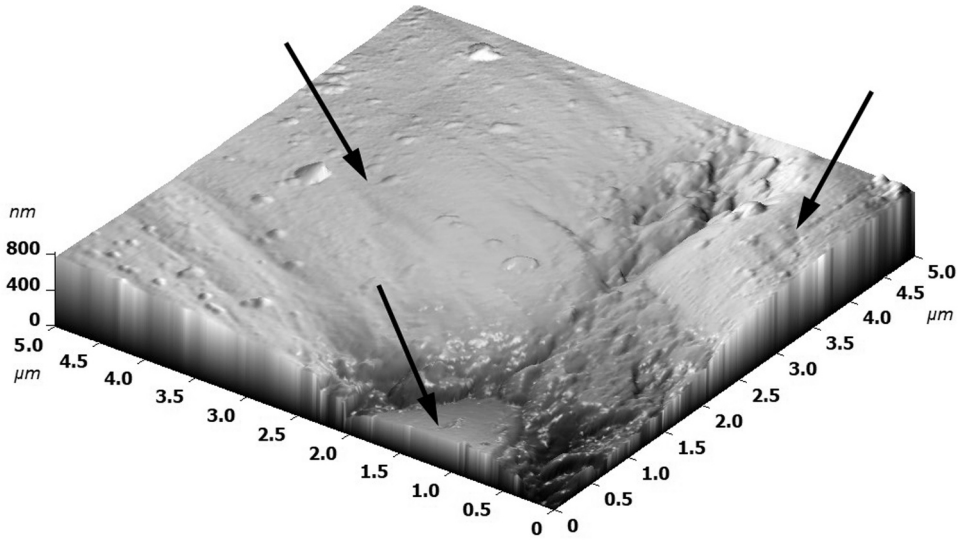

Fig. 3. AFM image of the 0.50-Hf ceramics surface.

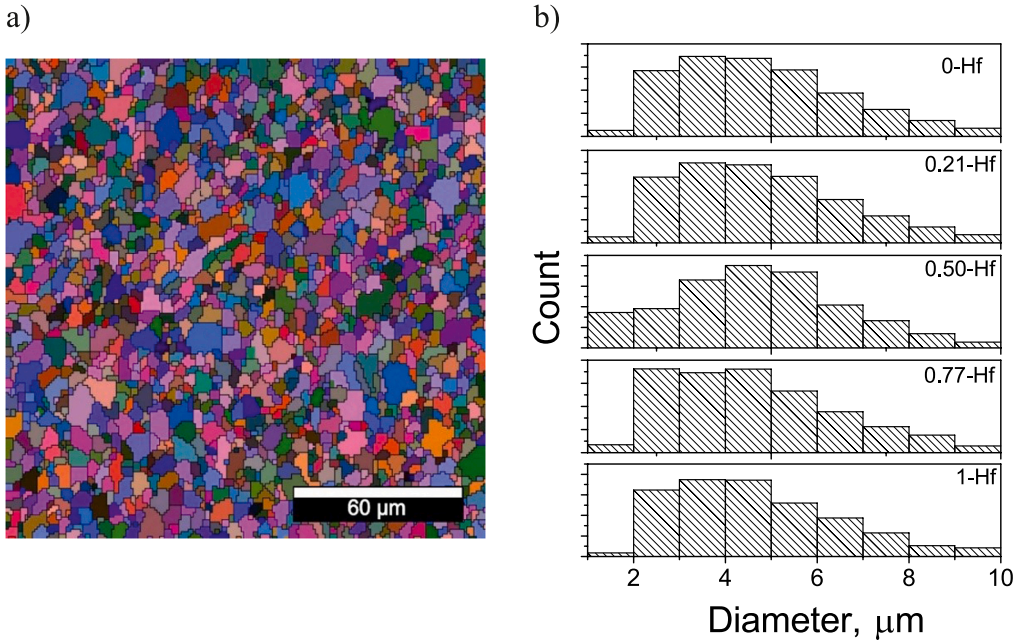

Fig. 4. a) EBSD image for the 0-Hf sample, b) histograms of grain size distribution for all samples.

that cubic ceramics of a given composition had been synthesized. A combination of AFM and EBSD studies demonstrated that the ceramics consist of large grains with a size of 2–8 μm and the space between them is filled with grains with a size of 100–400 nm. The linear dependence of the lattice parameter on the hafnium content indicates the formation of a solid solution.

3.2. Optical properties

3.2.1. Reflectance

Reflectance spectra were obtained for all samples. The absorption coefficient was calculated according to Kumar's model [47] using the formula:

$$\alpha(h\nu) = \frac{1}{2d} \ln \frac{R_{max} - R_{min}}{R_{h\nu} - R_{min}} \quad (1)$$

where R_{max} and R_{min} are maximum and minimum values of reflectance, d is the thickness of the absorption layer.

At the same time, the dependence of the absorption coefficient on the energy of the incident photons can be described by the power-law expression [48]:

$$\alpha(h\nu) \cdot h\nu = A\left(h\nu - E_g\right)^n \quad (2)$$

where A is a constant, E_g is the energy gap, n is the exponent that determines the type of interband transitions: 1/2 for direct transition and 2 for indirect.

The materials have been shown to have an indirect band gap (n=2). In order to obtain the energy gap values we carried out the analysis of spectral dependences of absorption determined Kumar's model in the coordinates of indirect optical transitions. Example of absorption spectrum for 1-Hf sample is shown in Fig. 5a. The optical band gap calculated for all samples is presented in Fig. 5b.

Fig. 5 shows the dependence of the optical band gap width on the

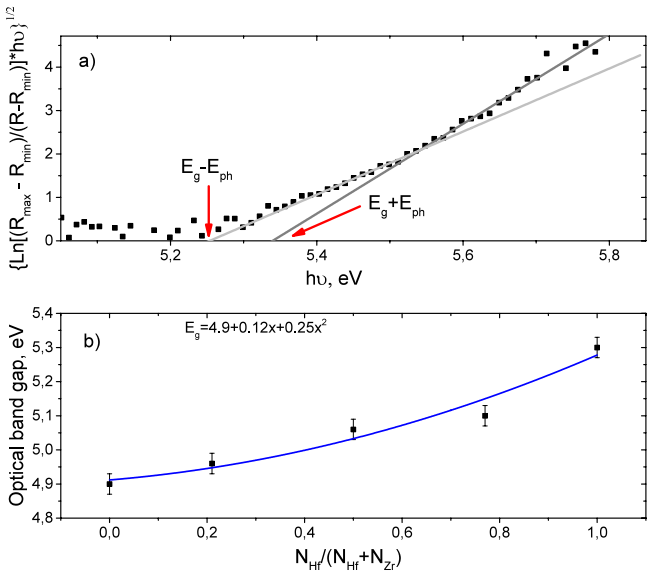

Fig. 5. a) Absorption spectrum of 1-Hf for indirect transitions in accordance with the Kumar's model [47]. The energy gap values (E_g) for transitions with absorption and emission of phonons (E_{ph}) are marked by arrows. b) Optical band gap dependence on hafnium content in the samples.

composition of the ceramic. The optical band gap depends on the ratio *x* as: E_g=4.9+0.12x+0.25x^2 (Fig. 5b). This result coincides with the conclusions in [49]. Other works, for example [50], give a different value of the band gap for ZrYO films - 5.7 eV. This scatter may be due to the presence of shallow trap levels, which can significantly shift the absorption edge.

3.2.2. Cathodoluminescence

CL spectra were obtained for all synthesized ceramics (Fig. 6).

The emission bands observed in the spectra were interpreted based on the work of K. Binnemans [51]. All CL bands were found to be associated with transitions in the Eu^{3+} ion. In particular, transitions from $^5D_2$ to $^7F_1$ level, from $^5D_1$ to $^7F_{1,3}$ level, and from $^5D_0$ to $^7F_{0,1,2,3,4}$ levels (see Fig. 6(b)) were observed in the CL spectra of all samples.

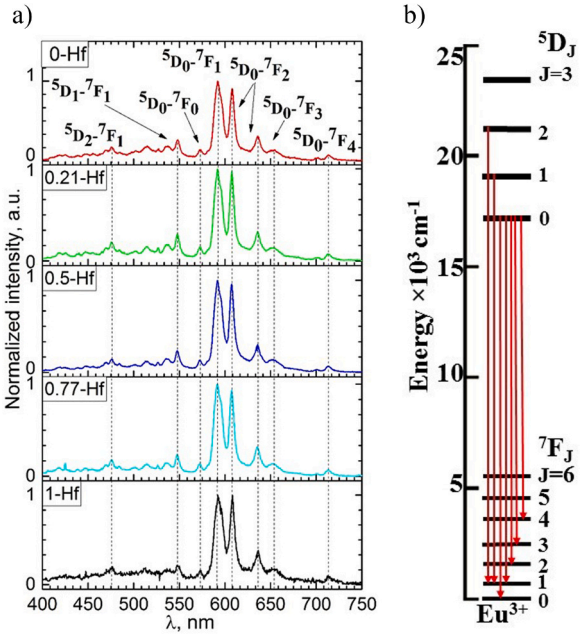

Fig. 6. a) CL spectra, b) scheme of Eu^{3+} luminescent transitions.

Analysis of the CL spectra confirmed that the ceramics were indeed stabilized in a cubic phase with a fluorite structure (f-ZrO_2, *Fm3m*). This is evidenced by the absence of the $^5D_0$ – $^7F_2$ Eu^{3+} transition band splitting [8]. In this crystalline phase, Eu^{3+} can be found in three nonequivalent positions: a position with D2d symmetry, which is formed by an environment of 8 oxygen atoms (CN8), a position with C1 symmetry, which has an oxygen vacancy in the second coordination shell, and a position with C3v symmetry, which has one oxygen vacancy in the first coordination sphere [8]. However, as shown in [40,52], with high-energy excitation it is impossible to identify local Eu^{3+} positions. It can be seen that the hafnium content does not affect the position and number of observed bands.

The decay times were obtained for the most intense $^5D_0$-$^7F_1$ transition. The obtained CL decay kinetics were approximated with good accuracy by the sum of two exponents:

$$I = I_0 + A_1\exp\left(-\frac{t}{\tau_1}\right) + A_2\exp\left(-\frac{t}{\tau_2}\right) \quad (3)$$

Parameters A_1 and A_2 provide information about the contribution of each exponent to the kinetics of luminescence decay while τ_1 and τ_2 are the characteristic luminescence decay times. The obtained parameter values are given in Table 2. The presence of two exponentials in luminescence decay is typical for ceramics. This is due to an increase in the probability of nonradiative transitions of activators located near grain boundaries [53].

3.2.3. Quantum yield, luminescence excitation spectra, and photoluminescence

As can be seen in Fig. 7, the quantum yield of the samples upon excitation of the $^7F_0$-$^5D_2$ transition does not depend on the hafnium content, and upon excitation of the $^7F_0$-$^5L_6$ transition, the highest quantum yield is observed in samples with the hafnium content, *x* from 0.21 to 0.77.

The excitation spectra of the $^5D_0$-$^7F_1$ transition of Eu^{3+} were obtained (Fig. 8). It was shown that the excitation spectra contain bands associated with intracenter transitions of Eu^{3+} and a charge transfer band (CTB). In contrast to cathodoluminescence spectra, transitions from high energy levels $^5D_1$ and $^5D_2$ are not observed.

The spectra were normalized to the magnitude of the $^7F_0$-$^5D_2$ transition, since the quantum yield upon excitation of this transition is similar for all studied samples (Fig. 7). The broad band with a maximum at 264 nm is the CTB for Eu^{3+}. It can be seen that the position of the CTB does not depend on the composition of the sample. The highest intensity of excitation of the $^5D_0$-$^7F_0$ Eu^{3+} transition is observed in the 0.21-Hf and 0.77-Hf samples.

3.2.4. Thermoluminescence

TL curves were obtained at heating rate of 0.25 K/s. TL curves have several intensive bands at temperatures of 150–250 K; however, for TL dosimetry, traps that emit at temperatures above 300 K and have a long lifetime at room temperature are of interest [54,55]. In the 0.50-Hf and 0.77-Hf samples, a separate band is observed with a maximum around 450–480 K (Fig. 9), which can be used as a dosimetric peak. In the 1-Hf sample such peak has a complex structure and consists of at least two bands.

Table2
CL decay times for the $^5D_0$-$^7F_1$ Eu^{3+} transition and contributions of exponents with different τ values.

Sample	A_1	τ_1, ms	A_2	τ_2, ms
0-Hf	0.59± 0.06	0.21± 0.02	0.41± 0.06	1.12 ± 0.06
0.21-Hf	0.57± 0.01	0.19 ± 0.01	0.43± 0.01	1.06 ± 0.02
0.50-Hf	0.61± 0.03	0.18 ± 0.02	0.39± 0.03	1.06 ± 0.06
0.77-Hf	0.56± 0.01	0.20 ± 0.01	0.44± 0.01	1.19 ± 0.04
1-Hf	0.63± 0.07	0.19 ± 0.01	0.37± 0.07	1.10 ± 0.02

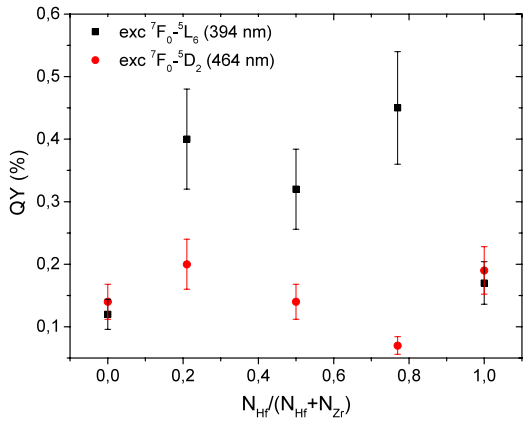

Fig. 7. Quantum yield of luminescence upon excitation of $^7F_0$-$^5D_2$ and $^7F_0$-$^5L_6$ transitions.

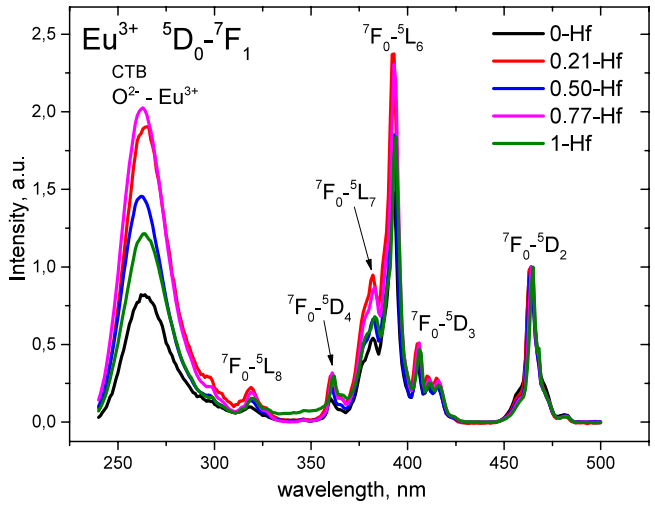

Fig. 8. Excitation spectra of the $^5D_0$-$^7F_1$ Eu^{3+} transition.

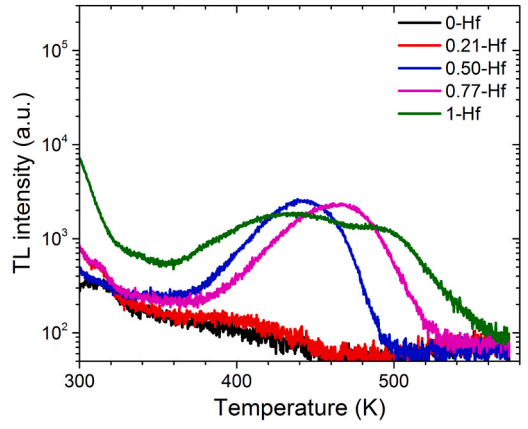

Fig. 9. Thermoluminescent curves obtained at heating rate of 0.25 K/s.

Several methods were utilized to determine activation energies of deep traps in 0.50-Hf, 0.77-Hf and 1-Hf samples. The first one proposed in [56,57] employs the shape of thermoluminescent curves. It was applied to 0.50-Hf and 0.77-Hf samples due to well isolated TL bands. The second one was used on 1-Hf sample and is based on various heating rates [56,58]. In this case heating rate was varied from 0.10 to 0.25 K/s and following equation was used:

$$\ln(I_m) \sim -\frac{E_a}{kT_m},$$

Where I_m and T_m are the intensity and temperature at peak maximum, and E_a is the activation energy. Both methods are generalized and do not require knowledge of the kinetic order [56]. The data (peak maximum temperature T_m and activation energies E_a) are presented in Table 3.

As can be seen from Table 3, there is no direct correlation between TL peak position and corresponding activation energy (E_a is higher in 0.50-Hf sample despite T_m being lower). This can be explained either by different frequency factors or by temperature lag which was unaccounted for.

Based on the literature data, it can be assumed that oxygen vacancies act as traps in these materials. In this case, it can be assumed that in the 0.50-Hf and 0.77-Hf samples, the traps are negatively charged oxygen vacancies V^- with the fourfold and with the threefold coordination [24]. In the 1-Hf sample, both of them are observed. Thus, the observed difference in thermoluminescence is associated with the Zr^{4+} and Hf^{4+} ratio. Another factor may be connected with higher refractory of HfO_2-based materials compared to ZrO_2-based materials [59,60]. Accordingly, under the selected annealing regime defects in the hafnium-free sample may be annealed, while in more refractory samples with a high hafnium content, similar defects may be not completely annealed.

4. Conclusions

Ceramic samples based on cubic zirconia-hafnia were successfully synthesized using starting precursors obtained by co-precipitation from common aqueous solutions. Minor phase admixture of does not exceed 1–2 wt%. Average grain size of zirconia-hafnia phases in ceramic matrix is about 4 μm but grains with an average size about 200 nm are present too. It was shown that a solid solution is formed over the entire range of compositions. The linear decrease of the lattice parameter as well as the dependence of the optical band gap on the composition were obtained. In the CL spectra, only bands associated with Eu^{3+} luminescence were observed. The number and position of bands associated with the $^5D_0$ - $^7F_1$ and $^5D_0$ - $^7F_2$ transitions confirm that the ceramics are stabilized in the cubic phase. It is shown that the hafnium content does not affect the position of the CL bands and the decay times of the $^5D_0$ - $^7F_1$ transition.

A complex study of the luminescent and thermoluminescent properties of the synthesized samples show that ceramics with hafnium content (x) from 0.5 to 0.8 are optimal for use in thermoluminescent dosimetry.

CRediT authorship contribution statement

Ekaterina V. Dementeva: Writing – original draft, Project administration, Funding acquisition. **Boris E. Burakov:** Writing – review & editing, Validation, Conceptualization. **Valentina V. Utochnikova:** Resources, Investigation. **Kseniia Orekhova:** Writing – review & editing, Investigation. **Azaliya A. Shakirova:** Visualization, Investigation. **Maria V. Zamoryanskaya:** Writing – review & editing, Validation, Supervision, Resources. **Maria A. Yagovkina:** Investigation. **Tatiana B. Popova:** Investigation. **Petr A. Dementev:** Writing – review & editing, Investigation. **Aleksey I. Lihachev:** Investigation. **Anatoliy F. Zatsepin:** Writing – review & editing, Resources. **Ivan D. Venevtsev:** Investigation. **Daniil S. Koshelev:** Investigation.

Table 3
Activation energies of deep traps for 0.50-Hf, 0.77-Hf and 1-Hf samples.

Sample	0.50-Hf	0.77-Hf	1-Hf	
T_m, K	429	486	438	500
E_a, eV	0.88±0.10	0.62±0.09	0.63±0.13	0.8±0.4

Declaration of Competing Interest

The authors declare that they have no known competing financial interests or personal relationships that could have appeared to influence the work reported in this paper.

Data Availability

Data will be made available on request.

Acknowledgments

The XRD and EBSD characterizations were performed using equipment owned by the Joint Research Center "Material science and characterization in advanced technology" (Ioffe Institute, St.-Petersburg, Russia).

Dementeva E.V., Dementev P.A., Orekhova K.N. and Shakirova A.A. thank the Russian Science Foundation support (grant 23-23-00465).

A.F. Zatsepin is grateful to the Ministry of Science and Higher Education of Russian Federation (project No. FEUZ-2023-0014).

References

[1] D.K. Smith, C.F. Cline, Verification of existence of cubic zirconia at high temperature (DOI:), J. Am. Ceram. Soc. 45 (1962) 249, https://doi.org/10.1111/j.1151-2916.1962.tb11135.x.

[2] P. Duwez, F.H. Brown, F. Odell, The zirconia-yttria system (DOI:), J. Electrochem. Soc. 98 (1951) 356, https://doi.org/10.1149/1.2778219.

[3] X. Hong, S. Xu, X. Wang, D. Wang, S. Li, B.A. Goodman, W. Deng, Growth, structure and optical spectroscopic properties of dysprosia-doped cubic yttria stabilized zirconia (YSZ) single crystals (DOI:), J. Lumin. 231 (2021) 117766, https://doi.org/10.1016/j.jlumin.2020.117766.

[4] X. Wang, X. Tan, S. Xu, F. Liu, B.A. Goodman, W. Deng, Preparation and up-conversion luminescence of Er-doped yttria stabilized zirconia single crystals (DOI:), J. Lumin. 219 (2020) 116896, https://doi.org/10.1016/j.jlumin.2019.116896.

[5] S. Stepanov, O. Khasanov, E. Dvilis, V. Paygin, D. Valiev, M. Ferrari, Luminescence performance of yttrium-stabilized zirconia ceramics doped with Eu^{3+} ions fabricated by spark plasma sintering technique (DOI:), Ceram. Int. 47 (2021) 6608, https://doi.org/10.1016/j.ceramint.2020.10.250.

[6] M.M. Eibl, S. Shaw, D. Prieur, A. Rossberg, M.C. Wilding, C. Hennig, K. Morris, J. Rothe, T. Stumpf, N. Huittinen, Understanding the local structure of Eu^{3+}- and Y^{3+}-stabilized zirconia: insights from luminescence and X-ray absorption spectroscopic investigations (DOI:), J. Mater. Sci. 55 (2020) 10095, https://doi.org/10.1007/s10853-020-04768-3.

[7] V.A. Kravets, K.N. Orekhova, M.A. Yagovkina, E.V. Ivanova, M.V. Zamoryanskaya, Eu^{3+} as a luminescent probe for studying the structure of R_2O_3 materials (R = Y, Eu, and Gd) (DOI:), Opt. Spectrosc. 125 (2018) 188, https://doi.org/10.1134/S0030400X18080167.

[8] E.V. Ivanova, V.A. Kravets, K.N. Orekhova, G.A. Gusev, T.B. Popova, M. A. Yagovkina, O.G. Bogdanova, B.E. Burakov, M.V. Zamoryanskaya, Properties of Eu^{3+}-doped zirconia ceramics synthesized under spherical shock waves and vacuum annealing (DOI:), J. Alloy. Compd. 808 (2019) 151778, https://doi.org/10.1016/j.jallcom.2019.151778.

[9] K. Smits, L. Grigorjeva, D. Millers, A. Sarakovskis, A. Opalinska, J.D. Fidelus, W. Lojkowski, Europium doped zirconia luminescence (DOI:), Opt. Mater. 32 (8) (2010) 827, https://doi.org/10.1016/j.optmat.2010.03.002.

[10] Z.G.Portakal Uçar, S. Akça, T. Doğan, Y.Z. Halefoğlu, Ü.H. Kaynar, M. Ayvacikli, J. G. Guinea, M. Topaksu, N. Can, Comprehensive study of photoluminescence and cathodoluminescence of Eu and Tb doped Mg_2SiO_4 prepared via a solid-state reaction technique (DOI:), Opt. Mater. 100 (2020) 109698, https://doi.org/10.1016/j.optmat.2020.109698 (2020).

[11] A. Aimi, H. Takahashi, K. Fujimoto, Afterglow properties and trap-depth control in ZrO_2:Ti, M (M = Ca^{2+}, Y^{3+}, Nb^{5+}, W^{6+}) (DOI:), Inorg. Chem. 59 (23) (2020) 16865, https://doi.org/10.1021/acs.inorgchem.0c01578.

[12] S. Mago, C. Sharma, P. Sharma, K.L. Singh, A.P. Singh, Comparative analysis of yttria stabilized zirconia (YSZ) and titania doped YSZ (YZT) sintered by two different routes: conventional and microwave processing (DOI:), Orient. J. Chem. 34 (5) (2018) 2539, https://doi.org/10.13005/ojc/340541.

[13] L.J. Espinoza-Pérez, E. López-Honorato, L.A. González, Development of ZrO_2 and YSZ coatings deposited by PE-CVD below 800 °C for the protection of Ni alloys (DOI:), Ceram. Int. 46 (10, Part A) (2020) 15621, https://doi.org/10.1016/j.ceramint.2020.03.109.

[14] K.-J. Hwang, M. Shin, M.-H. Lee, H. Lee, M.Y. Oh, T.H. Shin, Investigation on the phase stability of yttria-stabilized zirconia electrolytes for high-temperature electrochemical application (DOI:), Ceram. Int. 45 (7, Part B) (2019) 9462, https://doi.org/10.1016/j.ceramint.2018.09.026.

[15] A. Loganathan, A.S. Gandhi, Toughness evolution in Gd- and Y-stabilized zirconia thermal barrier materials upon high-temperature exposure (DOI:), J. Mater. Sci. 52 (2017) 7199, https://doi.org/10.1007/s10853-017-0956-2.

[16] L. Yang, D. Peng, X. Shan, F. Guo, Y. Liu, X. Zhao, P. Xiao, Oxygen quenching" in Eu-based thermographic phosphors: mechanism and potential application in oxygen/pressure sensing (DOI:), Sens. Actuators B 254 (2018) 578, https://doi.org/10.1016/j.snb.2017.07.092.

[17] H.S. Lokesha, M.L. Chithambo, A combined study of the thermoluminescence and electron paramagnetic resonance of point defects in ZrO_2:Er^{3+} (DOI:), Radiat. Phys. Chem. 172 (2020) 108767, https://doi.org/10.1016/j.radphyschem.2020.108767.

[18] M. Ťapajna, A. Rosová, K. Hušeková, F. Roozeboom, E. Dobročka, K. Fröhlich, Evidence of hafnia oxygen vacancy defects in MOCVD grown $Hf_xSi_{1-x}O_y$ ultrathin gate dielectrics gated with Ru electrode (DOI:), Microelectron. Eng. 84 (9–10) (2007) 2366–2369, https://doi.org/10.1016/j.mee.2007.04.052.

[19] E. Verrelli, D. Tsoukala, Investigation of the gate oxide leakage current of low temperature formed hafnium oxide films (DOI:), J. Appl. Phys. 113 (2013) 114103, https://doi.org/10.1063/1.4795278.

[20] G. Bersuker, J. Gavartin, J. Sim, C.S. Park, C. Young, S. Nadkarni, R. Choi, A. Shluger, B.H. Lee. Electron trapping processes in high-k gate dielectrics and nature of traps. 2006 International Symposium on VLSI Technology, Systems, and Applications, Hsinchu, Taiwan, 2006, p. 1. DOI: 10.1109/VTSA.2006.251087.

[21] V.A. Gritsenko, T.V. Perevalov, D.R. Islamov, Electronic properties of hafnium oxide: a contribution from defects and traps (DOI:), Phys. Rep. 613 (2015) 1, https://doi.org/10.1016/j.physrep.2015.11.002.

[22] V.A. Gritsenko, A.A. Gismatulin, Charge transport mechanism in La:HfO_2 (DOI:), Appl. Phys. Lett. 117 (2020) 142901, https://doi.org/10.1063/5.0021779.

[23] Y. Seo, S. Lee, I. An, C. Song, H. Jeong, Conduction mechanism of leakage current due to the traps in ZrO_2 thin film (DOI:), Semicond. Sci. Technol. 24 (2009) 115016, https://doi.org/10.1088/0268-1242/24/11/115016.

[24] D.R. Islamov, V.A. Gritsenko, T.V. Perevalov, V.A. Pustovarov, O.M. Orlov, A. G. Chernikova, A.M. Markeev, S. Slesazeck, U. Schröder, T. Mikolajick, G. Y. Krasnikov, Identification of the nature of traps involved in the field cycling of $Hf_{0.5}Zr_{0.5}O_2$ – based ferroelectric thin films (DOI:), Acta Mater. 166 (2019) 47, https://doi.org/10.1016/j.actamat.2018.12.008.

[25] M. Kurumada, H. Hara, E. Iguchi, Oxygen vacancies contributing to intragranular electrical conduction of yttria-stabilized zirconia (YSZ) ceramics (DOI:), Acta Mater. 53 (18) (2005) 4839, https://doi.org/10.1016/j.actamat.2005.06.027.

[26] K. Xiong, J. Robertson, M.C. Gibson, S.J. Clark, Defect energy levels in HfO_2 high-dielectric-constant gate oxide (DOI:), Appl. Phys. Lett. 87 (2005) 183505, https://doi.org/10.1063/1.2119425.

[27] D. Nakauchi, G. Okada, T. Yanagida, Scintillation, OSL and TSL properties of yttria stabilized zirconia crystal (DOI:), J. Lumin. 172 (2016) 61, https://doi.org/10.1016/j.jlumin.2015.11.028.

[28] S. Nikiforov, A. Dauletbekova, M. Gerasimov, Y. Kasatkina, O. Denisova, V. Lisitsyn, M. Golkovski, A. Akylbekova, A.-D. Bazarbek, A. Akilbekov, A. Popov, Thermoluminescent and dosimetric properties of zirconium dioxide ceramics irradiated with high doses of pulsed electron beam (DOI:), Crystals 13 (2023) 1585, https://doi.org/10.3390/cryst13111585.

[29] L. Sévin, V. Razafindramanana, A. Julian-Jankowiak, J.-F. Justin, F. Mauvy, F. Rebillat, Effect of high-content Yttria on the thermal expansion behaviour and ionic conductivity of a stabilised cubic Hafnia (DOI:), J. Eur. Ceram. Soc. 40 (15) (2020) 5859, https://doi.org/10.1016/j.jeurceramsoc.2020.05.044.

[30] S. Louise, A. Julian-Jankowiak, J.F. Justin, C. Langlade, P. Bertrand, N. Pelletier, Structural stability of hafnia-based materials at ultra-high temperature (DOI:), Mater. Sc. Forum 941 (2018) 1972, https://doi.org/10.4028/www.scientific.net/MSF.941.1972.

[31] C. Li, C. Ren, Y. Ma, J. He, H. Guo, Effects of rare earth oxides on microstructures and thermo-physical properties of hafnia ceramics (DOI:), J. Mater. Sci. Technol. 72 (2021) 144, https://doi.org/10.1016/j.jmst.2020.07.031.

[32] H. Yu, C. Liu, Z. Zhang, S. Huang, Y. Yang, R. Mao, H. Feng, J. Zhao, Single crystal growth and luminescent properties of YSH:Eu scintillator by optical floating zone method (DOI:), Chem. Phys. Lett. 738 (2020) 136916, https://doi.org/10.1016/j.cplett.2019.136916.

[33] E. Montes, P. Ceron, J. Guzmán-Mendoza, C. Falcony, M.Angel Vallejo, M. Antonio Sosa, Effect of europium concentration on the photoluminescent and thermoluminescent properties of HfO_2:Eu^{3+} nanocrystals (DOI:), Ceram. Int. 44 (7) (2018) 8081, https://doi.org/10.1016/j.ceramint.2018.01.250.

[34] C. Zhao, C.Zhou Zhao, S. Taylor, P.R. Chalker, Review on non-volatile memory with high-k dielectrics: flash for generation beyond 32 nm (DOI:), Materials 7 (2014) 5117, https://doi.org/10.3390/ma7075117.

[35] E.J. Shin, S.W. Shin, S.H. Lee, T.I. Lee, M.J. Kim, H.J. Ahn, J.H. Kim, W.S. Hwang, J. Lee, B.J. Cho, Capacitance boosting by anti-ferroelectric blocking layer in charge trap flash memory device (DOI:), IEEE Int. Electron Dev. Meet. (IEDM) (2020) 6.2.1, https://doi.org/10.1109/IEDM13553.2020.9371984.

[36] C. Jin, C.J. Su, Y.J. Lee, P.J. Sung, T. Hiramoto, M. Kobayashi, Study on the roles of charge trapping and fixed charge on subthreshold characteristics of FeFETs (DOI:), IEEE T. Electron Dev. 68 (3) (2021) 1304, https://doi.org/10.1109/TED.2020.3048916.

[37] E.V. Dementeva, P.A. Dementev, M.A. Yagovkina, M.V. Zamoryanskaya, Determination of type and concentration of traps in nanoscale-thick HfO_2 films applicable for gate dielectric stacks (DOI:), ACS Appl. Nano Mater. 6 (2023) 16212, https://doi.org/10.1021/acsanm.3c02178.

[38] Y. Cao, C. Li, Y. Ma, H. Luo, Y. Yang, H. Guo, Mechanical properties and thermal conductivities of 3YSZ-toughened fully stabilized HfO_2 ceramics (DOI:), Ceram. Int. 45 (3) (2019) 12851, https://doi.org/10.1016/j.ceramint.2019.03.208.

[39] D.R. Belichko, T.E. Konstantinova, A.V. Maletsky, G.K. Volkova, A. S. Doroshkevich, M.V. Lakusta, M. Kulik, A.A. Tatarinova, D. Mardare, C. Mita, N. Cornei, Influence of hafnium oxide on the structure and properties of powders

and ceramics of the YSZ–HfO_2 composition (DOI:), Ceram. Int. 47 (3) (2021) 3142, https://doi.org/10.1016/j.ceramint.2020.09.151.
[40] J. Dexpert-Ghys, M. Faucher, P. Caro, Site selective spectroscopy and structural analysis of yttria-doped zirconias (DOI:), J. Solid State Chem. 54 (2) (1984) 179, https://doi.org/10.1016/0022-4596(84)90145-2.
[41] G.A. Gusev, S.M. Masloboeva, M.A. Yagovkina, M.V. Zamoryanskaya, Synthesis and study of the luminescent properties of terbium-activated gadolinium tantalum-niobate (DOI:), Opt. Spectrosc. 130 (2) (2022) 265, https://doi.org/10.21883/EOS.2022.02.53221.2759-21.
[42] A.A. Shakirova, E.V. Dementeva, T.B. Popova, M.V. Zamoryanskaya, Characteristic properties of ceramics luminescence based on cubic $(Zr_{0.82-x}Hf_xY_{0.17}Eu_{0.01})O_{1.91}$ (DOI:), Opt. Spectrosc. 131 (5) (2023) 582, https://doi.org/10.21883/EOS.2023.05.56509.76-22.
[43] B.L. Adams, S.I. Wright, K. Kunze, Orientation imaging: the emergence of a new microscopy (DOI:), Met. Trans. 24A (1993) 819, https://doi.org/10.1007/BF02656503.
[44] R.D. Shannon, Revised effective ionic radii and systematic studies of interatomic distances in halides and chalcogenides (DOI:), Acta Cryst. A 32 (1976) 751, https://doi.org/10.1107/S0567739476001551.
[45] D. Araki, K. Kurosaki, H. Kimura, H. Muta, Y. Ohishi, K. Konashi, S. Yamanaka, Thermal and mechanical properties of hydrides of Zr–Hf alloys (DOI:), J. Nucl. Sci. Technol. 52 (2) (2015) 162, https://doi.org/10.1080/00223131.2014.935509.
[46] A. Neumann, V. Kahlenberg, I. Lerche, S. Stöber, H. Pöllmann, Synthesis and characterization of single crystal zircon-hafnon $Zr_{(1-x)}Hf_{(x)}SiO_4$ solid solutions and the comparison with the reaction products of a TEOS-based hydrothermal route (DOI:), ACS Omega 9 (14) (2024) 15781, https://doi.org/10.1021/acsomega.3c06960.
[47] V. Kumar, S. Kr. Sharma, T.P. Sharma, V. Singh, Band gap determination in thick films from reflectance measurements (DOI:), Opt. Mater. 12 (1999) 115, https://doi.org/10.1016/S0925-3467(98)00052-4.
[48] J. Tauc, Amorphous and Liquid Semiconductors, Plenum, New York, 1974, https://doi.org/10.1007/978-1-4615-8705-7.
[49] V.R. PaiVerneker, A.N. Petelin, F.J. Crowne, D.C. Nagle, Color-center-induced band-gap shift in yttria-stabilized zirconia (DOI:), Phys. Rev. B 40 (1989) 8555, https://doi.org/10.1103/PhysRevB.40.8555.
[50] N. Nicoloso, A. Löbert, B. Leibold, Optical absorption studies of tetragonal and cubic thin-film yttria-stabilized zirconia (DOI:), Sens. Actuators B. 8 (3) (1992) 253, https://doi.org/10.1016/0925-4005(92)85027-T.
[51] K. Binnemans, Interpretation of europium(III) spectra (DOI:), Coord. Chem. Rev. 295 (2015) 1, https://doi.org/10.1016/j.ccr.2015.02.015.
[52] M. Borik, A. Kulebyakin, V. Kyashkin, N. Larina, E. Lomonova, F. Milovich, V. Myzina, A. Nezhdanov, P. Ryabochkina, N. Tabachkova, E. Chernov, Structure and spectral luminescence properties of $(ZrO_2)_{0.909}(Y_2O_3)_{0.09}(Eu_2O_3)_{0.001}$ ceramics synthesized by uniaxial compaction and slip casting (DOI:), Materials 15 (2022) 7722, https://doi.org/10.3390/ma15217722.
[53] K. Orekhova, M. Zamoryanskaya, Decay kinetics in single crystals and ceramics based on yttrium aluminum garnet doped with rare earth ions (DOI:), J. Lumin. 251 (2022) 119228, https://doi.org/10.1016/j.jlumin.2022.119228.
[54] McKeever, S.W.S., Moscovitch, M., and Townsend, P.D. Thermoluminescence dosimetry materials: properties and uses. United Kingdom: N. p., 1995.
[55] S. Nikiforov, A. Dauletbekova, M. Gerasimov, Y. Kasatkina, O. Denisova, V. Lisitsyn, M. Golkovski, A. Akylbekova, A.-D. Bazarbek, A. Akilbekov, A. Popov, Thermoluminescent and dosimetric properties of zirconium dioxide ceramics irradiated with high doses of pulsed electron beam (DOI:), Crystals 13 (2023) 1585, https://doi.org/10.3390/cryst13111585.
[56] Pagonis V., Kitis G., Furetta C. Numerical and Practical Exercises in Thermoluminescence, ISBN-10: 0-387-26063-3 ISBN-13: 978-0387-26063-1, 2006.
[57] R. Chen, Glow curves with general order kinetics (DOI:), J. Electrochem. Soc. 116 (1969) 1254, https://doi.org/10.1149/1.2412291.
[58] R.K. Gartia, S. Ingotombi, T.S.G. Singh, P.S. Mazmudar, On the determination of the activation energy of a thermoluminescence peak by the two-heating-rates method (DOI:), J. Phys. D: Appl. Phys. 24 (1991) 65, https://doi.org/10.1088/0022-3727/24/1/011.
[59] R.P. Haggerty, P. Sarin, Z.D. Apostolov, P.E. Driemeyer, W.M. Kriven, L. Gauckler, Thermal expansion of HfO_2 and ZrO_2 (DOI:), J. Am. Ceram. Soc. 97 (7) (2014) 2213–2222, https://doi.org/10.1111/jace.12975.
[60] L. Audouard, M. Tsoutsouva, N. Horezan, E. Rimpot, J.-F. Justin, P. Bertrand, C. Langlade, M. Garcia, A. Julian-Jankowiak, Chemical and microstructural characterisation of HfO_2-Y_2O_3 ceramics with high amount of Y_2O_3 (33, 40 and 50 mol. %) manufactured using spark plasma sintering (DOI:), J. Eur. Ceram. Soc. 43 (5) (2022) 2093, https://doi.org/10.1016/j.jeurceramsoc.2022.12.061.